Determining fluid flow zones in a geothermal reservoir from thermal conductivity and temperature

Sébastien Haffen, Yves Géraud, Marc Diraison, Chrystel Dezayes

Determining fluid-flow zones in a geothermal sandstone reservoir from thermal conductivity and temperature logs

HAFFEN Sébastien (1), GERAUD Yves (1), DIRAISON Marc (1), DEZAYES Chrystel (2)

(1) Institut de Physique du Globe (IPG), UMR 7516 CNRS-Université de Strasbourg/EOST, 5 rue René Descartes, Strasbourg Cedex, 67084, France

(2) BRGM, Département Géothermie, BP36009, 3, avenue C. Guillemin, 45060 Orléans Cedex 2, France

Corresponding author: HAFFEN Sébastien, sebastien.haffen@eost.u-strasbg.fr,

Phone: 0033368850478

Abstract

A methodology of locating fluid-flow zones in a rock formation is applied to the Buntsandstein sandstone reservoir of borehole EPS1, Soultz-sous-Forêts, France. The method is based on analysing thermal gradients determined by two different methods for a same cored borehole, (1) from temperature log and (2) from thermal conductivity measures. Comparing the two thermal-gradient datasets reveals the fluid-circulation zones in the borehole. Using this approach, we identified three main hot-fluid circulation zones within the Buntsandstein sandstone, two controlled by sedimentary facies and one controlled by tectonic structures.

Keywords

Thermal gradient, thermal conductivity, permeability, sandstone reservoir, fluid circulation

1. Introduction

The decrease in fossil energy resources has led to an increase in demand for efficient utilization of unconventional and sustainable energy resources, such as geothermal reservoirs. Additionally, the increased obligation to reduce the environmental impact of exploiting conventional hydrocarbon resources has led to research into the geological storage of carbon dioxide. In this context of geothermal development and carbon dioxide storage within a sedimentary formation, one important aspect for the siting of future wells is to locate zones in which fluid circulation occurs. What is often overlooked, however, is the interpretation of temperature profiles (Chatelier et al., 2011), i.e. comparing the borehole temperature profile against the normal temperature increase induced by the local geothermal gradient. For a borehole in which no fluid circulation disrupts the thermal condition, the local geothermal gradient in the host rock is reflected by a steady temperature increase. Where the borehole intersects a local fluid flow zone, however, the vertical temperature distribution is disturbed (Keys, 1990). A well-known application of temperature measurements is for locating fluid 'feeder' and 'drainage' zones along a borehole by detecting rapid variations in the temperature profile with depth during the re-equilibrium phase (Barton et al., 1995; Bense et al., 2008; Khristoforova and Khristoforov, 2005; Trainer, 1968). Here we propose a new approach for locating fluid-flow zones based on analysing the thermal gradients in a borehole once thermal equilibrium is reached. The method compares two thermal gradients. The first is the thermal gradient in a rock formation which can be calculated with Fourier's law using the estimated heat-flow density at the bottom of the formation and the thermal conductivity measured on rock samples; this gives an estimated thermal gradient of the rock formation when heat-flow is controlled only by conduction and which take into account lithological heterogeneities. The second is the thermal gradient determined from temperature logs measured in the borehole; this corresponds to the real thermal gradient of the rock formation

derived by conduction from a deep heat source and also includes temperature disturbances due to the circulation of relative hot or cold fluids. Comparing the two thermal gradient datasets from a same well (Fig. 1a, b) enables one to determine the major possible fluid-flow zones.

We applied this method using the data from borehole EPS1 (Fig. 2) at the deep geothermal experimental site of Soultz-sous-Forêts (France) in the Upper Rhine Graben (Genter and Traineau, 1992). The borehole was cored continuously through the Buntsandstein, which here comprises variably argillaceous sandstone fractured by large faults, and a temperature log was recorded from the surface to 2200 m depth. Permeability measurements were also made on the borehole cores in order to compare the matrix permeability against the fluid-flow zones corresponding to the rock formation permeability. Comparing all these data makes it possible to determine what kind of permeability, matrix or fracture permeability, controls the fluid flow in the sandstone series.

2. Location and dataset

2.1. Location

The Soultz-sous-Forêts borehole EPS1 is located in the French part of the Upper Rhine Graben (Fig. 2a, b), near its western boundary marked by the major Rhine Fault. The graben, which is 30-40 km wide and extends NNE-SSW over a distance of 300 km, forms part of the western European Cenozoic Rift System. It is marked by a regional thermal anomaly strongly influenced by mantle uplift (Brun and Wenzel, 1991; Edel et al., 1975; Mueller et al., 1980; Wenzel et al., 1991) and its western border shows local thermal anomalies (Clauser et al., 2002) (Fig 2b). Consequently, the Buntsandstein in the Upper Rhine Graben has become a target for geothermal development (Dezayes et al., 2010).

Borehole EPS1, drilled through the sedimentary cover and into the basement (Fig. 2c), was cored continuously from a depth of 930 m, in the Muschelkalk limestone, to a depth of 2220 m in the Palaeozoic granite (Genter and Traineau, 1992; Vernoux et al., 1995). The cores therefore provide a continuous vertical section through the geothermal Buntsandstein sandstone reservoir between 1008.90 and 1416.77 m depth.

2.2. Depositional features and fracturing

According to *Ménillet et al.* (1989), the Buntsandstein consists of four stratigraphic units: the Annweiler Sandstone (*grès d'Annweiler*), Vosgian Sandstone (*grès vosgiens*), Intermediate Beds (*couches intermediaires*) and Voltzia Sandstone (*grès à Voltzia*). Other authors (Sizun, 1995a; Vernoux et al., 1995) have provided sedimentary descriptions of the cores from borehole EPS1 (Fig. 3a). Thus the basal Permian Sandstone (*Grès permiens*) (1416.77-1407.70 m) and Annweiler Sandstone (1407.70-1349.15 m) are composed of decimetre- to several metre thick facies sequences, medium- to fine-grained sandstones, interpreted as relatively distal braided fluvial networks in which sandy channels alternate with finer flood-plain and lacustrine deposits. The overlying Vosgian Sandstone (1349.15-1084.80 m) comprises two generally upward-fining units: the Lower Vosgian Sandstone (*Grès vosgiens inférieurs*) from the bottom of the unit to 1176.00 m, and the Upper Vosgian Sandstone (*Grès vosgiens supérieurs*) from 1176.00 m to the top of the unit. The Lower Vosgian Sandstone is made up of the Rehberg and Trifels beds consisting mainly of medium-grained sandstone sequences between one and several metres thick, and the Upper Vosgian Sandstone is composed of the Karlstal beds forming metre-thick medium- to coarse-grained sandstones sequences. *Bourquin et al.* (2009), propose a detailed stratigraphic column with genetic units based on a sedimentary and gamma-ray analysis (Fig. 3a, b) of the Vosgian Sandstone. They suggest that the Lower and Upper Vosgian Sandstone are made up of three sedimentary facies distinguished according to their mode of deposition (Fig. 3a): braided river

deposits within an arid alluvial plain (1349-1243 m; 1215-1183 m; 1112-1084 m), playa-lake deposits and fluvial and aeolian sand sheets (1183-1112 m), and fluvial-aeolian marginal erg deposits (1243-1215 m). The Intermediate Beds, located between 1084.80 and 1020.50 m, can be subdivided into four units from the base up: 1) the Obere Felsone (1084.80-1064.50 m) composed of metre-thick fluvial sandstone sequences, 2) the Bitche Conglomerate (*conglomérat de Bitche*; 1064.50-1060.00 m) consisting of micro conglomerate, 3) the Middle Intermediate Beds (*couches intermédiaires moyennes*; 1060.00-1044.00 m) made up of two upward-fining sequences, and 4) the Upper Intermediate Beds (*couches intermédiaires supérieures*; 1044.00-1020.50 m) beginning with a thin layer of conglomerate followed by a succession of thin upward-fining sandstone sequences. Globally, the Intermediate Beds reflect a braided fluvial system characterised by thinner and more differentiated sequences than the thick generally homogenous Vosgian Sandstone sequences. The Voltzia Sandstone, the uppermost formation of the Buntsandstein succession (1020.50-1008.90 m), is composed of beds several decimetres thick and reflects a transition to the lagoonal argillaceous deposits of the Muschelkalk. Buntsandstein sandstone are dominantly composed of lithic and feldspathic sandstones, the amount of clay allow the distinction between lower units (Annweiler sandstone and Permien Sandstone) and upper units (Intermediate Beds and Voltzia Sandstone) (Fig. 3b) (Vernoux, 1995). Buntsandstein Sandstone, from outcrops analysis, indicate a global composition of quartz (~80%), K-Feldspar (~20%) and micas (~1%) (Perriaux, 1961).

Natural fracturing was analysed on the continuous cores oriented using borehole imagery (Genter et al., 1997) (Fig. 4). The fracture trends were determined by the tectonic history of the Upper Rhine Graben area with a probable reactivation of some Hercynian structures (Illies, 1972; Illies, 1975; Rotstein et al., 2006; Schumacher, 2002; Villemin and Bergerat, 1987). A total of 325 fractures has been identified along the 408 m of core, with seven different fracture-density zones (Figs. 3d and 4): 1) 2.47 fract/m from 1008.90 to

1020.44 m, 2) 0.86 fract/m from 1020.44 to 1114.40 m, 3) 0.42 fract/m from 1114.40 to 1171.87 m, 4) 2.08 fract/m from 1171.87 to 1216.4 m, 5) 0.47 fract/m from 1216.40 to 1366.69 m, 6) 2.14 fract/m from 1366.69 to 1381.46 m, and 7) 0.26 fract/m from 1381.46 to 1416.77 m. The mean fracture density of the sedimentary sequence is 0.81 fract/m. The highly fractured zones (1), near the transition between the Muschelkalk and the Upper Buntsandstein, and (4) are both associated with the presence of major faulting (Vernoux et al., 1995), known as the Soultz Fault (Schnaebele, 1948) in the upper part of the borehole. The distribution of free fracture apertures (Figs. 3e and 4) and that of the fractures with depth (Vernoux et al., 1995) show a close relationship, with the largest free apertures being located within the high-density fracture zones. The vertical distribution of fracture azimuths (Fig. 4b) shows that the azimuths are fairly scattered in fracture zones 1, 2 and 5, and less scattered in zone 4 where a set of general N-S trends emerges. This set is also seen in fracture zone 6 and to a less extent in zones 3 and 7. The distribution of fracture dips with depth (Fig. 4a) is relatively stable. The fracture zones show steeply dipping values ranging from 42° to 88°, except in zone 1 and at the base of zone 5, where the fractures appear to be less inclined. The dips are equally balanced between east and west.

2.3. Drilling and borehole data

A temperature log (Fig. 3c), undisturbed by technical drilling operations such as mud circulation was run in borehole EPS1 in November 1991 nine months after the drilling, was completed and when the well was at thermal equilibrium. The logging technique was a continuous analogue measurement using a 4-wire cable with a PT1000 sensor (*Schellschmidt* (2011), personal communication). The log gives temperature data for each metre through the sandstone, with temperatures ranging from 120.24 °C at the top of the Buntsandstein (1009.19 m) to 136.45 °C at the bottom (1415.95 m). The mean geothermal gradient in this part of the

borehole is 39.85 °C/km. Fluid loss during the drilling operation had been noted at around 1200, 1215, 1230 and 1370 m.

2.4. Thermal conductivity and permeability measurements on core samples

At least three techniques exist for measuring the thermal conductivity of rocks: i.e. the divided-bar steady-state technique, the needle-probe transient technique and the optical scanning technique (Popov et al., 1999; Sass et al., 1971; Sass et al., 1984). In this study we used the optical scanning technique because its ease of use enabled us to rapidly obtain a large number of measurements. The method is based on scanning a black-primed sample surface with a mobile constant and continuously operated heat source in combination with two infrared temperature sensors (Popov, 1999). The heat source and the trailing temperature sensors move at the same relative speed along the core sample, maintaining a constant distance from one another and from the analysed surface. The trailing temperature sensors continuously register the value of the maximum temperature increase along the heating line for each measurement and so provide a continuous thermal conductivity profile. The size of the heating spot is 1 mm and the relative measurement error is about 3% of the measured value. Knowing the temperature rise, the strength of the heat source, the distance between the heat source and the temperature sensors, and the thermal conductivity of two standards, one is able to determine the thermal conductivity of each sample along the scanning line.

The thermal conductivity of the core samples was measured under saturated conditions. For this, the samples were initially dried to a constant weight at 60 °C, and then saturated by submerging them in distilled water inside a sealed vacuum chamber for 48 hours. The thermal conductivity of the water-saturated samples was then measured perpendicular

($\lambda_{\perp}$) to the bedding in a direction parallel to the vertical heat-flow. A total of 77 cores were measured (Table 1).

The thermal conductivities measured on the cores perpendicular to the stratification (Table 1) range between 2.21 and 5.95 W/(mK) (respectively in the Annweiler Sandstone and the Upper Vosgian Sandstone) with a mean value of 3.84±0.16 W/(mK). The Annweiler Sandstone and Voltzia Sandstone exhibit the lowest mean thermal conductivities of 3.30±0.24 W/(mK) and 3.23±1.08 W/(mK), respectively. With the Vosgian Sandstone, the upper part has a specific mean thermal conductivity that is higher than in the lower part (4.53±0.58 W/(mK) for the Upper Vosgian Sandstone, and 4.01±0.19 W/(mK) for the Lower Vosgian Sandstone). In the Intermediate Beds, the Obere Felsone and Upper Intermediate Beds returned similar mean thermal conductivity values of 3.82±1.03 W/(mK) and 3.81±0.43 W/(mK), respectively; the lowest values (3.66±0.42 W/(mK)) were in the Middle Intermediate Beds. The two Bitche Conglomerate samples returned 4.72 W/(mK) and 3.43 W/(mK).

In situ permeability measurements along all the cores of borehole EPS1 were performed using a portable Tiny-perm II air minipermeameter (Fig. 3g), which provides reliable permeability values in the 1 mD to 10 D range. The measurement is performed by squeezing a rubber nozzle (inner diameter: 10 mm; outer diameter: 24 mm) against the sample surface and withdrawing the air from the permeameter with a single stroke of a syringe. As air is pulled into the sample, a micro-controller unit simultaneously monitors the syringe volume and the transient vacuum pulse created at the sample surface (*Tiny Perm User's Manual*). In all, 1112 measurements were made parallel to the stratification along the cores, giving approximately one measurement every 35 cm, with each site being carefully and gently

brushed to remove dust prior to the permeability measurement. In order to validate the measurements obtained with the portable air minipermeameter, the results were compared with permeability data obtained by *Sizun* (1995b) using a classic laboratory constant-head gas permeameter with nitrogen as fluid; Sizun's measurements were performed on cylindrical samples (length: 6 cm; diameter: 2 cm) drilled from the borehole cores, both parallel and perpendicular to the stratification. Our air permeability values proved to be close to the gas permeability values (Fig 3g). Moreover, both measurement methods enable one to determine the matrix permeability taking into account structures smaller than a few centimetres.

Permeability measurements performed on the cores of borehole EPS1 (Table 2) range over three orders of magnitude, from 0.1 mD to 0.5 D. Several kinds of section are distinguished along the cores (Fig. 3g and Table 2); those with relatively stable intermediate permeability values ranging from 0.66 mD to 8.77 mD, and four zones with large permeability value variations: 1) values from 181.53 to 0.34 mD from the base of the Vosgian Sandstone to 1300 m, reflecting a global upward trend with depth; 2) values between 0.63 and 512.68 mD, with a mean of 40.48 mD, in the Fluvio-aeolian marginal erg facies; 3) values between 0.35 and 387.24mD, with a mean of 38.25 mD indicating high heterogeneity and a downward trend between the Upper and Lower Vosgian Sandstone contact and 1120 m in the Playa lake facies; and 4) values globally increasing from 0.81 to 87.52mD, with mean value of 11.81 mD, in the Obere Felsone .

3. Method Description

3.1. Heat-flow density

Heat-flow density (q in mW/m²) is determined from the product of the thermal conductivity (λ in W/(mK)) and the temperature gradient (dT/dz in °C/km) according to Fourier's law (1-D case), Eq. (1):

$$q = -\lambda \times dT/dz \quad (1)$$

The heat-flow density in the basal unit of borehole EPS1 represents the heat-flow entering the sedimentary series from the granitic basement and is assumed to be constant across the sandstone reservoir in a system considered to be conductive. The heat production rate in the Buntsandstein sandstone is about 1 $\mu W/m^3$ (Schellschmidt and Clauser, 1996) because of the low amount of disintegrable radioactive elements. This cumulative contribution is ignored in the heat-flow density calculation.

The heat-flow density in the basal Permian sandstone was determined according to Fourier's law (Eq. 1) using the interval method (Powell et al., 1988) whereby the heat-flow density is calculated from the thermal gradient and thermal conductivity. In the present case the thermal gradient was calculated as the average of the measured thermal gradients in the borehole intersecting the Permian unit (29.76±1.44 °C/km), and the mean thermal conductivity (3.17±0.47 W/(mK)) was calculated from $\lambda_{\perp}$ measured on the cores and corrected from the in situ temperature according to the law proposed by *Vosteen and Schellschmidt* (2003) (Table 1). Based on the above thermal-gradient and thermal-conductivity values, the calculated heat-flow density through the basal unit gives a value of about 94 mW/m².

3.2. Thermal gradient determined from thermal conductivity measurements on cores and Fourier's law

The thermal gradient was calculated for each core depth along the Buntsandstein series from the measured thermal conductivity, corrected for in situ temperature, and knowledge of

the heat-flow density determined above. The values range from 19.77 to 50.31 °C/km across the Buntsandstein, with a mean value of 31.38±1.28 °C/km (Fig. 3f).

3.3. Thermal gradient determined from temperature log data

The thermal gradient was also calculated from the temperature log data (Fig. 3f). It appears relatively constant and low in the lower part of the sedimentary series (thermal gradient through the Permian Sandstone: 29.99 °C/km) and increases upward toward the top of the Buntsandstein sandstone reservoir (thermal gradient through the Voltzia Sandstone: 71.15 °C/km). The thermal gradient maxima within the Lower Vosgian Sandstone (~1220 m deep) and Upper Vosgian Sandstone (~1120 m deep) are around 48 and 59 °C/km respectively.

4. Results

A number of authors suggest that fluid circulation in the Upper Rhine Graben, from the granitic basement to the overlying Mesozoic formations, induces heat transfer by conduction and convection or advection (Aquilina et al., 1997; Clauser and Neugebauer, 1991; Clauser and Villinger, 1990; Flores Marquez, 1992; Pribnow and Clauser, 2000; Pribnow and Schellschmidt, 2000; Rybach, 2007; Schellschmidt and Clauser, 1996). In order to identify these flow zones we compared theoretical thermal gradients induced by the conductive flux against measured thermal gradients induced by conductive and convective transfer. The theoretical thermal gradient (or calculated gradient) was obtained using the heat-flow density calculated at the bottom of the sedimentary series and the thermal conductivity measured on core samples; it is indicative of the conductive part of the heat-flow. This calculated gradient is fairly constant, with some variations induced by different thermal conductivities of the different sedimentary facies. The measured thermal gradient (or

measured gradient) was determined from the temperature profile run in the borehole, and presents several variation zones. Comparing the calculated and measured thermal gradient profiles reveals two cases (Fig. 3f). The one is where the values in the calculated and measured gradients are equal, which indicates that the heat transfer is governed mainly by conduction and that there is no significant occurrence of hot fluid flow. The other case is where the measured gradient gives higher values than the calculated gradient, which leads one to suspect the presence of hot fluid circulation.

From the sandstone/granite interface to 1235 m depth, both the measured and calculated thermal gradients indicated similar values (Fig. 3f); the average measured gradient obtained from the temperature logs is 33.11±0.26 °C/km (ranging between 26.26 and 45.45 °C/km), and the average calculated gradient is 32.98±1.66 °C/km (ranging between 26.54 and 50.31 °C/km). These variations result from the thermal conductivity variations of the different sedimentary facies described in this part of the sedimentary sequence (Fig. 3a and Table 1), and so the heat transfer in this interval is apparently governed only by conduction without any hot fluid circulation. Between 1235 and 1190 m in the borehole, the measured gradients are higher than the calculated ones; the average measured gradient obtained from the temperature logs is 40.37±1.37 °C/km, whereas the average calculated gradient is 27.06±2.37 °C/km. This large difference between the two values could be the result of hot fluid circulation in this part of the borehole. Then from 1190 to 1150 m, the two gradients are again similar, indicating that the heat transfer is again controlled mainly by conduction. The observation of zones in which both thermal gradients indicate same values and encircling a hot flowing zone, involve that this hot fluid don't disturb the heat-flow of the surrounding formations. Thus, in this case, hot fluid circulation zones can't be assimilating to massive heat production zones. The lack of measurements between 1150 and 1130 m prevents us from determining precisely the nature of the heat exchanges for this depth interval; nevertheless, the measured gradients deduced from

the temperature logs increase to values in excess of 40.00 °C/km as against around 30.00 °C/km associated with the conductive flux, and so we can assume that hot fluid circulation occurs in this depth interval. From 1080 m to the top of the formation, the measured gradient increases gradually to a maximum of 85.15 °C/km in the upper Buntsandstein. At the same time, the calculated gradient associated with the conductive flux remains below 40.00 °C/km (apart from the last two values near the top at 42.89 and 48.08 °C/km) indicating low thermal conductivity values (Table 1). These observations suggest a decreasing influence of conduction in the heat transfer from a depth of 1180 m toward the top of the Buntsandstein and thus an increasing contribution of hot fluid circulation toward the top of the sandstone formation.

5. Discussion

Comparing the macroscopic flow/non-flow zones, deduced from the thermal gradient analysis, against the matrix permeability measurements on the one hand and the sedimentary facies and fracture dispersion along the core on the other, allows us to determine what components control the hot fluid circulation. Four main situations are depicted: 1) zones with no indication of heat or fluid transfer (i.e. the thermal gradient curves are quite similar) and with low measured permeability values; 2) zones with no indication of heat or fluid transfer and with high permeability values; 3) zones with an indication of heat or fluid transfer and with high permeability values; and 4) zones with an indication of heat or fluid transfer and with low permeability values. Each of these is discussed below.

Different fluid pathways may occur. For example, open fractures can provide good drainage for fluid circulation (Caine et al., 1996); they define a large-scale permeability but without effect on the matrix structure, which is a transfer property not described by our

permeability measurements. Another pathway can be formed by the porosity network at matrix scale and be controlled by sedimentary or diagenetic processes or by microfissures; the permeability of these small-scale networks is measurable with a portable air minipermeameter. In the cases described below we have combined these two kinds of structures to explain our results in term of the porous network or fluid pathway.

Non-flow zones (NFZ)

The non-flow zones are characterized by similar values for a) thermal gradients calculated from thermal conductivity measurements and reflecting conductive heat flux, and b) thermal gradients measured from the borehole temperature profile and reflecting conductive and convective heat flux. Three such zones were localized in borehole EPS1 (Fig. 3f): 1) at the top of the Playa lake level *(NFZa)*, 2) at the bottom of the Playa lake level *(NFZb)*, and 3) in the bottom part of the formation *(NFZc)*, from 1235 m depth to the granite/sandstone contact. The first two zones are relatively thick and also associated with low permeability levels. The third zone *(NFZc)* incorporates the Permian Sandstone, the Annweiler Sandstone and the first unit of Braided river facies in the Lower Vosgian Sandstone (Fig. 3a). The lower part of this third zone is characterized by high permeability values (Fig. 3g), whereas the Annweiler Sandstone, Permian Sandstone and upper part of the first unit of braided river facies have relative low permeability values (Table 2). This particular relationship could be induced by the macroscopic sedimentary facies with crossbeds and thick clayey beds forming a complex network of impermeable layers that strongly reduces the macroscopic permeability even though the matrix permeability is high. The highly fractured zone 6 in the Annweiler Sandstone (Fig. 3d) consists mainly of sealed fractures with a few fractures showing small free apertures (Fig. 3e) that are insufficient for a network connection to the hot fluid feeding area.

Flow zones

The flow zones are characterized by measured thermal gradients (deduced from the temperature logs) that are higher than the calculated thermal gradients determined from the thermal conductivity. Three main flow zones are recognized from the top down (Fig. 3f): 1) at the top of the Buntsandstein *(FZa)*; 2) in the Playa lake facies between 1130 and 1150 m *(FZb)*; and 3) in the second Braided river facies and the underlying Fluvio-aeolian marginal erg facies between 1190 and 1235 m *(FZc)*. Although *FZa* is composed of relative low permeability sandstone (Table 2), except in the Obere Felsone, the Buntsandstein in this part of the borehole is marked by the highly fractured zone 1 and the upper part of zone 2 (Fig. 3d) with many open fractures (Fig. 3e). Moreover, the fracture zones near the transition between the Muschelkalk and the Upper Buntsandstein are associated with the presence of a major fault and its damage zone (Fig. 5). Thus it is through fractures that the deep hot fluid source feeds this flow zone. *FZb* is characterized by high matrix permeability values (Table 2) and a very few sealed fractures (Fig. 3e); it is thus controlled mainly by sedimentary or diagenetic properties and is connected with the deep hot fluid sources through the westward-developed fault damage zone (Fig. 5). For *FZc*, the bottom part in the fluvio-aeolian marginal erg facies (Fig. 3a) has a high matrix permeability (Table 2) and a few sealed fractures (Fig. 3e), whereas the top, in the braided river facies, has a relative low matrix permeability (Table 2) and a high fracture density (fracture zone 4, Fig. 3d) with many large free apertures (Fig. 3e) forming the damage zone developed around a major fault zone. The open fractures in the fault zone would appear to form a pathway for the deep hot fluids, enabling them to flow widely into the underlying permeable Fluvio-aeolian facies (Fig. 5).

Fracturing

The open fracture azimuths controlling the flow zone at the top of the Buntsandstein formation are fairly scattered (Fig. 4c), corresponding to the brittle deformation associated with the major fault damage zone. The orientation of the open fractures in fracture zone 6, corresponding to a non-flow zone, is globally N-S (Fig. 4c) and could be described as a fracture corridor activated during the Oligocene opening of the Upper Rhine Graben. The orientation of the open fractures in the second fault zone, corresponding to the flow zone of fracture zone 4, is rather scattered, but with many of the fractures again showing a global N-S orientation (Fig. 4c). It would thus appear that every open fracture near the two major fault zones, regardless of the strike, are channels for hot fluid flow. The deeper fracture zones are farther from the major faults (Fig. 5) and it would appear that, with depth, the globally N-S-striking open fractures are less well, or not at all, supplied with hot fluid from the major fault zone. Consequently it would be open fractures with other orientations that channel the hot fluid in the deeper flow zones.

Conceptual model

Analysis of the thermal gradients in borehole EPS1 has enabled us to locate permeable zones where hot fluid flows occur at formation scale in the Buntsandstein. Nevertheless different pathways are needed to explain the observed thermal gradient anomalies (Fig. 5). For example, an upward-flowing path for these fluids from the deep part of the basin is provided by fault zones. The damage zones associated with the faults would also enable the upward flowing fluids to connect with the stratigraphic reservoirs (‘horizontal layers’). Such transfer paths to the stratigraphic reservoirs are controlled mainly by sedimentary and diagenetic processes. The reservoirs have high matrix permeability and an excellent horizontal connectivity and are formed by the Playa Lake and Fluvio-aeolian marginal erg facies. Conversely the braided river facies, despite high matrix permeability, present a broad network of thick oblique argillaceous layers which decreases the macroscopic permeability.

The flow paths thus appear as a composite network controlled by ‘sedimentary’ permeability on one hand and by ‘fracture’ permeability on the other. Fracturing associated with the two fault zones is used by the upward flowing fluids to connect with usable stratigraphic levels characterized by high matrix permeability with no impermeable macroscopic layers. This is why the Playa Lake and Fluvio-aeolian marginal erg facies provide a suitable reservoir that could be easily be connected to a deep hot fluid source.

6. Conclusion

A methodology, based on thermal gradient analysis, is presented for locating hot fluid flow in a rock formation. The method involves determining the thermal gradient from thermal conductivity measurements on core samples and also from borehole temperature logs run in the same borehole. With a heat-flow density calculation and thermal conductivity measurements, one can apply Fourier's law to calculate the thermal gradient in a rock system where the heat transfer is assumed to be controlled only by conduction and thus taking into account lithological heterogeneities. The thermal gradient calculated from a measured temperature log profile takes into account both the conductive and the convective or advective part due to fluid circulation. On the one hand, if the thermal gradient deduced from temperature logs indicates similar values to the thermal gradient calculated with Fourier's law, the heat transfer is assumed to be controlled solely by conduction in the rock formation and thus involves no relative hot or cold fluid circulation. If, on the other hand, the thermal gradient deduced from the temperature logs indicates higher or lower values than that calculated with Fourier's law, then respectively hot or cold fluid flow could be suspected.

We applied this method to borehole EPS1 (Soultz-sous-Forêts, Upper Rhine Graben) for which temperature logs and core samples from the Buntsandstein are available. Variations

between the two determined thermal gradient curves revealed three main hot fluid flow levels alternating with non-flow zones in the sandstone formation. The pattern was then compared against the fracture distribution, and also against sedimentological analyses determined from the borehole cores, in order to determine the driving components of the fluid flows. The flow zones in the Buntsandstein are controlled on the one hand by a macroscopic network with two major fault zones providing a flow path for the deep heat source and on the other hand by a matrix network formed during sedimentary or diagenetic processes within the Playa-lake and Fluvio-aeolian marginal erg facies. At another level in the Buntsandstein sequence, the sedimentary braided river formations may have high matrix permeability, but would not support a macroscopic fluid flow; this is due to their macroscopic sedimentary structure of thick oblique clayey layers that drastically reduce the level's connectivity and thus its permeability.

The proposed method can be used to identify the major fluid-flow levels or structures. Comparing the macroscopic and microscopic data is helpful in determining the relative contribution of the two networks on fluid flow at formation scale.

Acknowledgment

The authors would like to thank EEIG Heat Mining and A. Genter, the scientific coordinator, for providing the borehole EPS1 data and allowing access to the cores. We are also grateful to ADEME (French Agency for Environment and Energy) and BRGM (French Geological Survey) which provided financial support for this work in the framework of the joint CLASTIQ (CLAyed sandSTone In Question) project.

References

Aquilina, L., Pauwels, H., Genter, A. and Fouillac, C., 1997, Water-rock interaction processes in the Triassic sandstone and the granitic basement of the Rhine Graben: Geochemical investigation of a geothermal reservoir. Geochimica Et Cosmochimica Acta, 61: 4281-4295.

Barton, C., Zoback, M. and Moos, D., 1995, Fluid flow along potentially active faults in crystalline rock. Geology, 23: 683-686.

Bense, V., Person, M., Chaudhary, K., You, Y., Cremer, N. and Simon, S., 2008, Thermal anomalies indicate preferential flow along faults in unconsolidated sedimentary aquifers. Geophysical Research Letters, 35: 6.

Bourquin, S., Guillocheau, F. and Peron, S., 2009, Braided rivers within an arid alluvial plain (example from the Lower Triassic, western German Basin): recognition criteria and expression of stratigraphic cycles. Sedimentology, 56: 2235-2264.

Brun, J.P. and Wenzel, F., 1991, Crustal-scale structure of the southern Rhine Graben from ECORS-DEKORP seismic-reflection data. Geology, 19: 758-762.

Caine, J.S., Evans, J.P. and Forster, C.B., 1996, Fault zone architecture and permeability structure. Geology, 24: 1025-1028.

Chatelier, M., Ruelleu, S., Bour, O., Porel, G. and Delay, F., 2011, Combined fluid temperature and flow logging for the characterization of hydraulic structure in a fractured karst aquifer. Journal of Hydrology, 400: 377-386.

Clauser, C. and Villinger, H., 1990, Analysis of conductive and convective heat-transfer in a sedimentary basin, demonstrated for the Rheingraben. Geophysical Journal International, 100: 393-414.

Clauser, C. and Neugebauer, J., 1991, Thermisch relevante Tiefenwasserzirculation in der Oberkruste unter dem Oberrheingraben ? Eingrenzungen mit Hilfe hydrothermischer Modellrechnungen Geologie Jahrbuch, E48: 185-217.

Clauser, C., Griesshaber, E. and Neugebauer, H.J., 2002, Decoupled thermal and mantel helium anomalies: implication for the transport regime in continental regime rift zones. Journal of Geophysical Research, 107: 2269.

Dezayes, C., Thinon, I., Courrioux, G., Haffen, S. and Bouchot, V., 2010, Toward a better knowledge of the Lower Triassic reservoir in the Upper Rhine Graben, Bali, Indonesia.

Edel, J.B., Fuchs, K., Gelbke, C. and Prodehl, C., 1975, Deep structure of southern Rhinegraben area from seismic refraction investigations. Journal of Geophysics-Zeitschrift Fur Geophysik, 41: 333-356.

Flores Marquez, E.L., 1992, Transfert de chaleur et de masse en milieu sédimentaire et fracturé. Modélisation numerique de la convection naturelle autour du site geothermique de Soultz (Graben du Rhin) Thesis, Institut National Polytechnique de Lorraine, France: 267 p.

Genter, A. and Traineau, H., 1992, Borehole EPS1, Alsace, France: Preliminary geological results from granite core analysis for Hot Dry Rock research. Scientific Drilling, 3: 205-214.

Genter, A., Castaing, C. and Martin, P., 1997, Assessment of reservoir fracturing from boreholes: Comparison between core and wall-image data. Revue de l'institut Francais du Pétrole, 52: 45-60.

Genter, A., Guillou-Frottier, L., Breton, J.P., Dezayes, C., Egal, E., Feybesse, J.L., Goyeneche, O., Nicol, N., Quesnel, F., Quinquis, J.P., Roig, J.Y. and Schwartz, S.,

2004, Typologie des systemes HDR/HFR en Europe. Final report. BRGM/RP-53452-FR: 165p., 175 fig., 110 tab.

Illies, H., 1972, The Rhine Graben rift system - plate tectonic and transform faulting. Geophysical Survey, 1: 27-60.

Illies, H., 1975, Recent and paleo-intraplate tectonic in stable Europe and the Rhinegraben rift system. Tectonophysics, 29: 251-264.

Keys, W.S., 1990, Borehole geophysics applied to ground-water investigations. In: USGS (Ed.), Techniques of Water-Resources Investigations of the United States Geological Survey, Book 2: pp 150.

Khristoforova, N. and Khristoforov, A., 2005, Fluid migration and location of fractured layers in the crystalline basement by temperature logging in the Volga Region, Russia. Journal of Geochemical Exploration, 89: 187-190.

Ménillet, F., Coulombeau, C., Geisser, F., Konrad, H.J. and Schwoerer, P., 1989, Notice explicative, *Carte géologique. France*, Feuille Lembach, 168, Orléans. Ed. BRGM: 91 p.

Mueller, S., Ansorge, J., Egloff, R. and Kissing, E., 1980, A crustal cross section along the Swiss Geotravers from the Rhinegraben to the Po Plain. In: Rybach L, Lamber A (eds) Symposium on the Alpin geotravers with special emphasis on the Basel-Chiasso profile. Eclogae Geologicae Helveticae, 73: 463-483.

Perriaux, J., 1961, Contribution à la géologie des Vosges gréseuses. Mémoire du Service de Carte Géologique d'Alsace et de Lorraine, 18: 236 p.

Place, J., Diraison, M., Naville, C., Geraud, Y., Schaming, M. and Dezayes, C., 2010, Decoupling of deformation in the Upper Rhine Graben sediments. Seismic reflection and diffraction on 3-component Vertical Seismic Profiling (Soultz-sous-Forets area). Comptes Rendus Geoscience, 342: 575-586.

Popov, Y.A., Pribnow, D.F.C., Sass, J.H., Williams, C.F. and Burkhardt, H., 1999, Characterization of rock thermal conductivity by high-resolution optical scanning. Geothermics, 28: 253-276.

Powell, W.G., Chapman, D.S., Balling, N. and Beck, A.E., 1988, Continental Heat-flow density. In: Haenel, R., Stegena, L., Rybach, L. (Eds). Handbook of Terrestrial Heat-flow Density Determination. 504 p, 167-222.

Pribnow, D. and Clauser, C., 2000, Heat and fluid flow at the Soultz hot dry rock system in the Rhine Graben. Proceeding World Geothermal Congress: 6 p.

Pribnow, D. and Schellschmidt, R., 2000, Thermal tracking of upper crustal fluid flow in the Rhine Graben. Geophysical Research Letters, 27: 1957-1960.

Rotstein, Y., Edel, J.B., Gabriel, G., Boulanger, D., Schaming, M. and Munschy, M., 2006, Insight into the structure of the Upper Rhine Graben and its basement from a new compilation of Bouguer Gravity. Tectonophysics, 425: 55-70.

Rybach, L., 2007, The geothermal conditions in the Rhine Graben - a summary. Bulletin für Angewandte Geologie, 12/1: 29-32.

Sass, J.H., Lachenbruch, A.H. and Munroe, R.J., 1971, Thermal conductivity of rocks from measurments on fragments and its application to heat-flow determinations. Journal of Geophysical Research, 76: 3391-3401.

Sass, J.H., Stone, C. and Munroe, R.J., 1984, Thermal conductivity determination on solid rock - a comparison between steady-state divided bar apparatus and a commercial transient line-source device. Journal of Volcanology and Geothermal Research, 20: 145-153.

Schellschmidt, R. and Clauser, C., 1996, The Thermal Regime of the Upper Rhine Graben and the Anomaly at Soultz Zeitschrift für Angewandte Geologie, 42: 40-44.

Schnaebele, R., 1948, Monographie géologique du champ pétrolifère de Pechelbronn. Mémoire du service géologique d'Alsace Lorraine, Strasbourg, 7: 254p.

Schumacher, M.E., 2002, Upper Rhine Graben: Role of preexisting structures during rift evolution. Tectonics, 21.

Sizun, J.P., 1995a, Modification des structures de porosité de grès lors de transformations petrographiques dans la diagenese et l'hydrothermalisme Thèse, Institut de Geologie. Strasbourg, Université Louis Pasteur, Strasbourg, France: 297 p.

Sizun, J.P., 1995b, Modification des structures de porosite de gres lors de transformations petrographiques dans la diagenese et l'hydrothermalisme Thesis, Inst. Geol. Strasb., Université Louis Pasteur, Strasbourg, France.

Trainer, F.W., 1968, Temperature profile in water wells as indicators of bedrocks fracture. USGS, Professional Paper, 600-B, Washington.

Vernoux, J.F., Genter, A., Razin, P. and Vinchon, C., 1995, Geological and petrophysical parameters of a deep fractured sandstone formation as applied to geothermal exploitation, EPS-1 borehole, Soults-sous-Forêts, France. BRGM Open file Report, R 38622: 69 p.

Villemin, T. and Bergerat, F., 1987, L'évolution structurale du fossé Rhénan au cours du Cénozoïque : un bilan de la déformation et des effets thermiques de l'extention Bulletin de la Société Geologique de France III, (2): 245-255.

Vosteen, H.D. and Schellschmidt, R., 2003, Influence of temperature on thermal conductivity, thermal capacity and thermal diffusivity for different types of rock. Physics and Chemistry of the Earth, 28: 499-509.

Wenzel, F., Brun, J.P., Blum, R., Bois, C., Burg, J.P., Coletta, B., Durbaum, H., Durst, H., Fuchs, K., Grohmann, N., Gutscher, M.A., Hubner, M., Karcher, T., Kessler, G., Klockner, M., Lucazeau, F., Luschen, E., Marthelot, J.M., Meier, L., Ravat, M.,

Reichert, C., Vernassat, S. and Villemin, T., 1991, A deep reflexion seismic line across the northern Rhine graben. Earth and Planetary Science Letters, 104: 140-150.

Figures

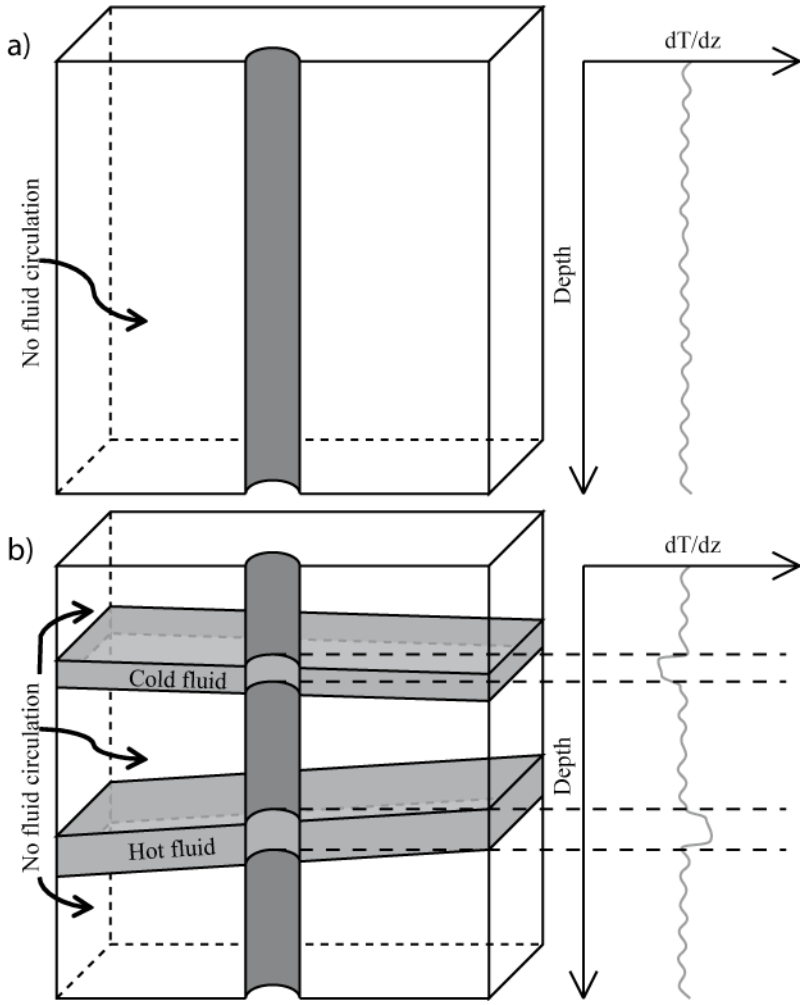

Figure 1. **a)** Schematic representation of the thermal gradient measurable in a borehole intersecting a rock formation with no fluid circulation. Variations in the thermal gradient are caused by lithological variations, and heat transfer is induced by conductive processes. **b)** Schematic representation of the thermal gradient in the same rock formation, but where hot and cold fluid flows occur at different levels; heat input and output induce 'positive' and 'negative' variations in the gradient.

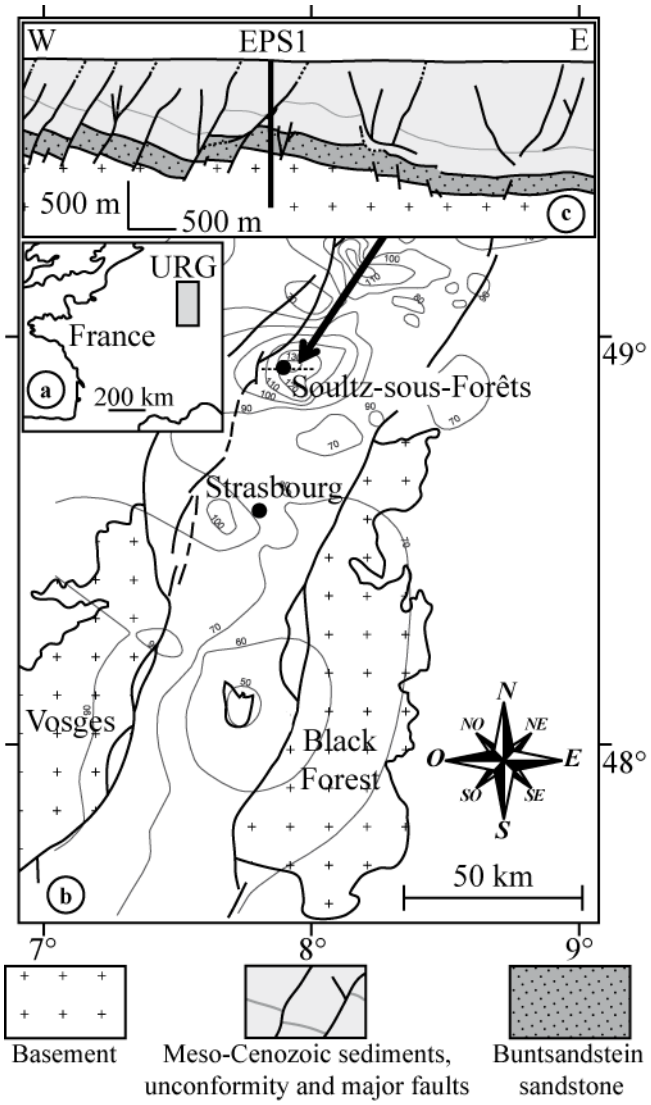

Figure 2. **a)** Location of the Upper Rhine Graben (URG) in Western Europe. **b)** URG map (modified from *Schumacher* (2002)); the black dot and small black dotted line locate borehole EPS1 and the geological cross-section (c) respectively; the grey lines indicate the temperature at 1500 m depth based on data from GGA Hannover (Genter et al., 2004; Pribnow and Schellschmidt, 2000). **c)** Soultz-sous-Forêts geological cross-section (redrawn after *Place et al.* (2010)) showing the approximate location of borehole EPS1 at depth.